bioRxiv preprint doi: https://doi.org/10.1101/2025.08.20.671067; this version posted August 25, 2025. The copyright holder for this preprint (which was not certified by peer review) is the author/funder, who has granted bioRxiv a license to display the preprint in perpetuity. It is made available under a CC-BY 4.0 International license.

Title: **Mechanical energetic contributions of the rectus femoris during perturbed walking**

Running Title: Rectus femoris perturbation energetics

Authors: *Pawel R. Golyski[a,b], Gregory S. Sawicki[a,b,c,d]

Affiliations:

[a] Parker H. Petit Institute for Bioengineering and Biosciences, Georgia Institute of Technology, Atlanta, GA, USA

[b] George W. Woodruff School of Mechanical Engineering, Georgia Institute of Technology, Atlanta, GA, USA

[c] Institute for Robotics and Intelligent Machines, Georgia Institute of Technology, Atlanta, GA, USA

[d] School of Biological Sciences, Georgia Institute of Technology, Atlanta, GA, USA

*Corresponding Author.

E-mail: pgolyski3@gatech.edu

ORCID

Pawel R. Golyski: 0000-0001-9844-2859

Gregory S. Sawicki: 0000-0002-5588-6297

Abstract Word Count: 210

Word Count: 6029

Number of Figures/Tables: 6, 3 Supplementary

Number of References: 84

bioRxiv preprint doi: https://doi.org/10.1101/2025.08.20.671067; this version posted August 25, 2025. The copyright holder for this preprint (which was not certified by peer review) is the author/funder, who has granted bioRxiv a license to display the preprint in perpetuity. It is made available under a CC-BY 4.0 International license.

Abstract: Animals maintain locomotor stability following external perturbations by coordinating muscular responses to produce desired mechanical behavior at different levels of description (*e.g.*, muscle-tendon units, joints, legs). To investigate the role of proximal musculature in responding to perturbations during human walking, here we extend a previous analysis relating joint and leg levels down to the level of the rectus femoris. Using *in-vivo* B-mode ultrasound processed with a custom automated fascicle tracking application and EMG measurements to drive Hill-type models of muscle force, we investigated mechanical energetics of the rectus femoris in 7 individuals who experienced rapid, transient unilateral belt accelerations during walking. We hypothesized that: H1) the rectus femoris would actively lengthen on the perturbed leg during the perturbed stride and H2) on the contralateral leg the rectus femoris would reflect the mechanical energetic demand at the knee and leg levels. H1 was partially supported, with the rectus femoris fascicles being decoupled from muscle-tendon unit lengthening. H2 was not supported, with the rectus femoris best reflecting the energetic role of the hip, as opposed to the knee or leg. Overall, these findings provide a first estimate of the variety of roles proximal muscles play in maintaining stability and lay the groundwork for additional *in-vivo* measurement informed multi-scale analyses of perturbed locomotion.

Keywords: stability, biomechanics, deep learning, B-mode ultrasound, muscle dynamics

bioRxiv preprint doi: https://doi.org/10.1101/2025.08.20.671067; this version posted August 25, 2025. The copyright holder for this preprint (which was not certified by peer review) is the author/funder, who has granted bioRxiv a license to display the preprint in perpetuity. It is made available under a CC-BY 4.0 International license.

Introduction

As animals move through their environments, they exhibit an impressive ability to maintain stability despite external mechanical disturbances (*e.g.*, rocks, sidewalks, ice). The high-level goal of maintaining a locomotor trajectory is accomplished through stabilizing responses mediated by 1) feedforward strategies (*e.g.*, foot placement (1,2)), 2) feedback mechanisms (*e.g.*, reflexes (3,4)]), and 3) intrinsic mechanical properties of biological structures (*e.g.*, muscle-tendon interactions (5–7)). While stabilizing mechanical responses have been studied at different levels of musculoskeletal description (*e.g.*, center of mass [COM], legs, joints, muscles), relating responses *across* different levels remains difficult. To address this challenge, a paradigm was recently developed which used mechanical energy to both quantify the explicit energetic demand of a perturbation and to serve as a "common currency" with which to relate responses across different levels of musculoskeletal description in humans (8).

This approach leveraged the idea that during level split-belt treadmill walking, if both belts are moving at the same constant speed, both the net work performed by each leg on the COM and the corresponding treadmill belt must be zero over a stride on average, so the net work performed by the overall leg (*i.e.*, the sum of both COM and treadmill contributions), must be zero as well (9,10). Barring modeling inaccuracies, this overall leg work should be equal to the sum of the work of all lower limb joints (11). In (8), transient increases in unilateral belt speed were targeted to either early or late stance to perturb the flow of mechanical energy. In this non-steady state condition, net mechanical work was performed by each leg on the COM and the corresponding treadmill belt. The difference between these non-steady state overall leg and joint level mechanical work contributions and their corresponding steady state values constituted the mechanical energetic demand of the perturbation. By relating changes in joint and overall leg work, this approach allowed for investigation of which joints best reflected leg level demands. For the perturbed leg, on both the perturbed and first recovery stride, changes in ankle (vs. knee or hip) work best reflected changes in overall leg work, in agreement with literature from speed and ground height changes (12–16). However, on the contralateral leg, the knee strongly reflected overall leg level demands, spanning both net positive and negative work during the perturbed stride. This finding suggested proximal joints and muscles of the leg may play an important role in mediating transient energetic demands.

The goal of this work is to extend the perturbation energetics paradigm and investigate the role of proximal leg musculature in responding to rapid unilateral belt accelerations. As there is currently no gold-standard approach to quantifying human *in-vivo* fascicle lengths of proximal muscles during

bioRxiv preprint doi: https://doi.org/10.1101/2025.08.20.671067; this version posted August 25, 2025. The copyright holder for this preprint (which was not certified by peer review) is the author/funder, who has granted bioRxiv a license to display the preprint in perpetuity. It is made available under a CC-BY 4.0 International license.

dynamic tasks, to accomplish our overarching goal we developed a custom automated application which leveraged deep-learned models for aponeurosis detection in conjunction with fascicle detection based on other recent fascicle tracking algorithms (17,18) to estimate fascicle lengths from B-mode ultrasound images. These fascicle lengths were used together with *in vivo* muscle activations to estimate fascicle and MTU forces (19), in addition to the respective mechanical powers. Of the quadriceps and hamstring muscles, we focused our analysis on the rectus femoris because 1) we sought to determine whether the extension of the perturbed limb by the perturbation would be apparent at the level of proximal muscle fascicles, as opposed to being buffered by series elasticity (7,20), and 2) an increased knee extensor moment is a major feature of the recovery strategy on the contralateral leg following a belt acceleration during walking (21). Since proximal muscles are considered to have less compliant tendons relative to distal muscles (22,23), our first hypothesis (H1) was that the rectus femoris would actively lengthen on the perturbed leg during the perturbed stride, resulting in increased negative fascicle and MTU power and work relative to steady state. On the contralateral leg, because the knee reflected overall leg level energetic demands (8), and the functional behavior of the rectus femoris fibers and MTU (predominantly damper-like; (24)) is more similar to the knee than the hip (predominantly motor-like; (15)), our second hypothesis was that the rectus femoris would reflect contralateral knee energetic demands and therefore also overall leg energetic demands.

bioRxiv preprint doi: https://doi.org/10.1101/2025.08.20.671067; this version posted August 25, 2025. The copyright holder for this preprint (which was not certified by peer review) is the author/funder, who has granted bioRxiv a license to display the preprint in perpetuity. It is made available under a CC-BY 4.0 International license.

Methods

Experimental Protocol

Data were collected from 7 healthy able-bodied individuals (5 males, 2 females, mean [SD]: 25 [2] years, 178.5 [12.1] cm stature, 72.7 [13.3] kg) as part of a study investigating leg and joint level energetics (8). Participants walked on an instrumented split-belt treadmill (CAREN, Motek, Netherlands), and after 5 minutes of acclimation at 1.25 m s^{-1} (25), experienced rapid (15 m s^{-2} acceleration), transient (~340 ms duration, ~33% of the perturbed gait cycle) increases in unilateral belt speed (1.25 m s^{-1} to 2.5 m s^{-1}) targeted to either early or late stance (Figure 1). The algorithm by which these perturbations were delivered is described elsewhere (26). Each participant experienced 40 total perturbations in a randomized order (both legs, early and late stance onset timings, and 10 repetitions of each leg/timing combination), with 30-40 steps between perturbations to allow for return to steady state walking (27). All participants (recruitment period: 8/28/2020 - 3/6/2021) provided written informed consent and all protocols were approved by the Institutional Review Board at the Georgia Institute of Technology (Protocol H20163). The sample size was determined based on pilot data indicating a sample of 6 participants would be capable of detecting a significant ($p < 0.05$) effect of speed on average fascicle length over a stride in proximal leg muscles with 82% power.

External Kinematics and Kinetics

Ground reaction forces were collected at 2000 Hz from an instrumented split-belt treadmill (CAREN, Motek, Netherlands). A full-body marker set consisting of 67 retroreflective markers (modified Human Body Model 2; (28)]) was used to track bony landmarks and body segments (head, hands, forearms, upper arms, torso, pelvis, thighs, shanks, and feet). Marker trajectories were collected at 200 Hz using a 10-camera motion capture system (Vicon; Oxford, UK). For each participant, a generic full-body musculoskeletal model (22 segments, 37 degrees of freedom; (29)) was scaled in OpenSim 4.0 (30) using a static standing trial to generate a participant-specific model. The metatarsophalangeal and subtalar joints were locked to treat the foot as a rigid body. All trials were manually inspected to ensure crossover steps were removed from analysis, leaving 222 successful trials. Joint angles were calculated from marker trajectories using the OpenSim Inverse Kinematics tool. Joint moments were calculated with the OpenSim Inverse Dynamics tool using both joint angles and ground reaction forces applied to the calcanei of the scaled models. Time-varying moment arms of the rectus femoris to the hip and knee

bioRxiv preprint doi: https://doi.org/10.1101/2025.08.20.671067; this version posted August 25, 2025. The copyright holder for this preprint (which was not certified by peer review) is the author/funder, who has granted bioRxiv a license to display the preprint in perpetuity. It is made available under a CC-BY 4.0 International license.

joints in addition to MTU lengths and velocities were calculated using the OpenSim Muscle Analysis tool using joint angles and the scaled models. Kinematic and kinetics were low-pass filtered using 4th order zero-phase Butterworth filters with cutoff frequencies of 6 and 15 Hz, respectively. Strides were segmented using a 30 N threshold applied to vertical ground reaction force.

Leg and Joint Energetics

Joint mechanical powers were calculated as the product of joint angular velocities (obtained by differentiating joint angles with respect to time) and joint moments. Mechanical powers of each leg were calculated using a modified individual limbs method (11,31) as the sum of 1) power flowing from each leg to the COM, 2) power flowing from each leg to the treadmill, and 3) peripheral power of the leg segments moving relative to the COM of the whole body. Leg to COM power was calculated as the dot product of the corresponding ground reaction force and COM velocity. COM velocity was calculated as the time derivative of COM position from the Body Kinematics tool in OpenSim using both joint angles and scaled models. Leg to treadmill power was calculated as the product of anteroposterior leg force (equal and opposite to ground reaction force) and treadmill velocity (collected at approximately 70 Hz). Peripheral leg power was quantified by adding together the time derivatives of the rotational and translational components of kinetic energy of the leg segments (11,32,33) as calculated from inertial estimates from the scaled models and segment velocities from the OpenSim Body Kinematics tool.

Electromyography

Surface electromyography (EMG) was collected at 2000 Hz (Avanti, Delsys, Natick, MA) from 7 lower limb muscles of the left leg: the rectus femoris (RF), tibialis anterior, soleus, medial gastrocnemius, vastus medialis, biceps femoris, and gluteus maximus. EMG sensors were placed on the bellies of each muscle following light abrasion of the skin surface. All EMG envelopes were calculated by first high-pass filtering EMG signals using a 10 Hz zero-phase Butterworth filter, then full-wave rectifying the signal, then low-pass filtering the signal with a 30 Hz zero-phase Butterworth filter (34,35). Signal offsets were first removed by subtracting the minimum envelope value during a relaxed static trial. These demeaned envelopes were then normalized by the difference between the maximum within-participant envelope value across all perturbations and the minimum resting value, similar to previous work (34,36). To estimate muscle activations, this normalized signal was then passed through first-order dynamics (37) with an activation time constant of 35 ms, and a deactivation time constant of 58 ms, corresponding to a mixed fiber type muscle (19), which is applicable to the RF (38). Since the RF is the

bioRxiv preprint doi: https://doi.org/10.1101/2025.08.20.671067; this version posted August 25, 2025. The copyright holder for this preprint (which was not certified by peer review) is the author/funder, who has granted bioRxiv a license to display the preprint in perpetuity. It is made available under a CC-BY 4.0 International license.

primary muscle of interest in this work, activations of other muscles are included as a supplementary figure (Figure S1).

Ultrasonography

B-mode cine ultrasound images were collected at approximately 115 Hz from the RF of the right leg using an ArtUS EXT-1H acquisition unit and a 60 mm long LV8-5N60-A2 probe (Telemed, Vilnius, LT). The probe was placed over the muscle belly at a consistent longitudinal location to the RF EMG sensor on the left leg. The probe was aligned such that fascicles and both superficial and deep aponeuroses could be clearly visualized. The imaging angle of the probe was also varied in EchoWave software (Telemed, Vilnius, LT) to provide the best contrast of the fascicles and aponeuroses – between 0 and -10 degrees based on the participant. An external trigger was used to synchronize motion capture and ultrasound image timestamps.

bioRxiv preprint doi: https://doi.org/10.1101/2025.08.20.671067; this version posted August 25, 2025. The copyright holder for this preprint (which was not certified by peer review) is the author/funder, who has granted bioRxiv a license to display the preprint in perpetuity. It is made available under a CC-BY 4.0 International license.

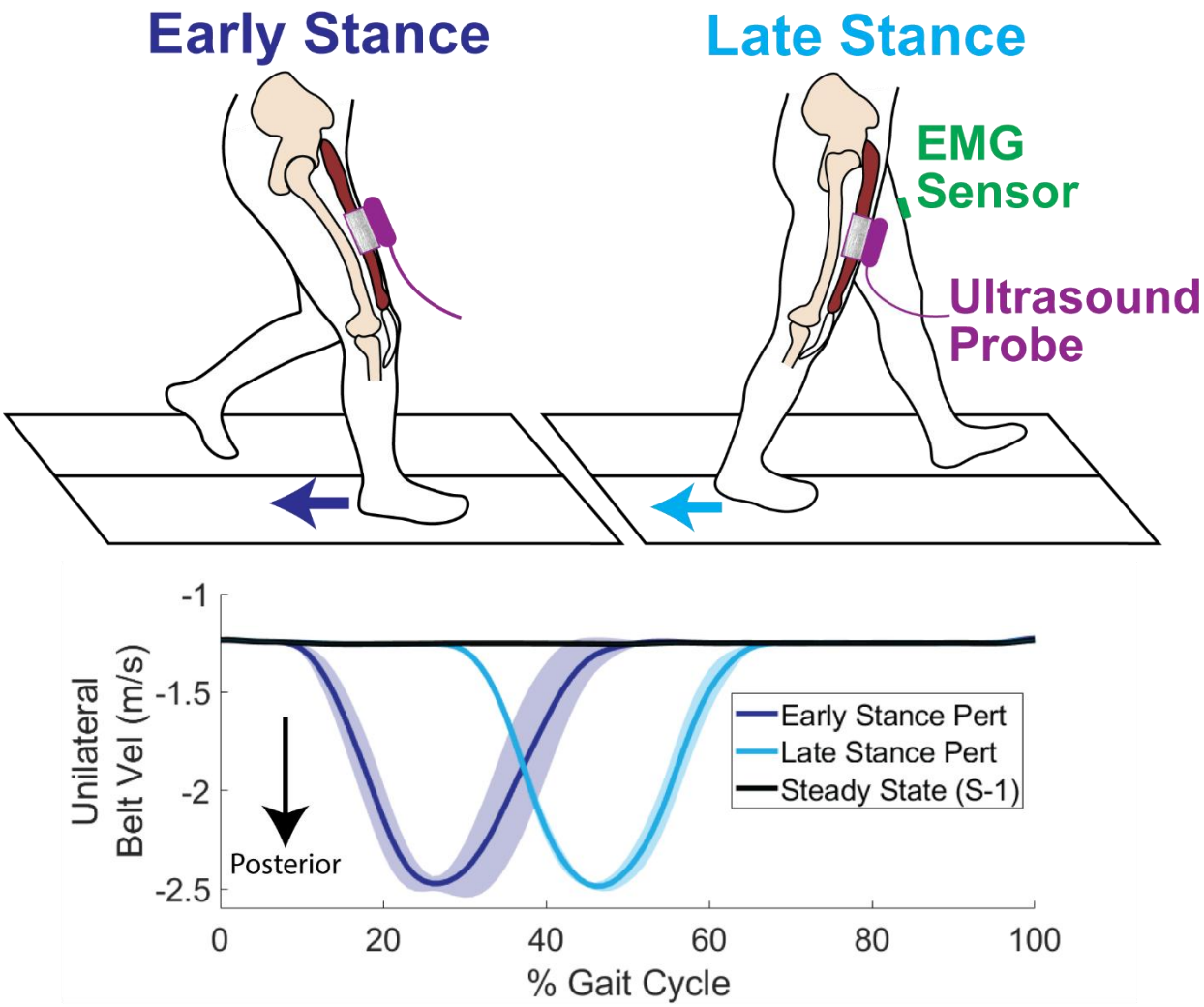


Figure 1 – Conceptual overview of the treadmill perturbation and muscle-level measurements. Unilateral treadmill belt velocity traces show across-subject ensemble averages. Shaded regions represent ±1 standard deviation.

Custom Ultrasound Tracking Application

A custom application was developed in Matlab R2019b (Mathworks, Natick, MA, USA) to estimate proximal muscle fascicle lengths and pennation angles from B-mode ultrasound images during dynamic tasks. The application consists of two parts. Part 1 involves training study-specific deep-learned models for detection of superficial and deep aponeuroses. Part 2 uses the identified aponeurosis locations to define a region of interest and estimates representative fascicle parameters from hyperechoic "snippets" of fascicles within that region. The application workflow is shown in Figure 1B.

bioRxiv preprint doi: https://doi.org/10.1101/2025.08.20.671067; this version posted August 25, 2025. The copyright holder for this preprint (which was not certified by peer review) is the author/funder, who has granted bioRxiv a license to display the preprint in perpetuity. It is made available under a CC-BY 4.0 International license.

Part 1 – Aponeurosis Identification using Deep-Learning

Part 1 of the application consists of 3 steps. First, an image set is generated to train and validate deep-learning models for identification of superficial and deep aponeuroses. The overarching design strategy of this approach is to "overfit" models to perform best on the remaining images of a study. This approach allows for rapid training of models with a small dataset on a mid-range desktop computer and avoids having to collect and manually track a data set that generalizes across tasks, probes, participants, etc. (39). The drawback of this approach is that the trained models are likely study specific, limiting reproducibility. In this study, a set of 490 images was used for training and validating models. This image set consisted of 35 frames equally spaced in time across 1 perturbed gait cycle from both the ipsilateral and contralateral legs for all 7 participants. From the identified set of images, the superficial and deep aponeuroses are then manually traced to produce binary masks (roipoly, Matlab). The second step is training separate models for identification of pixels belonging to either superficial or deep aponeuroses. Both the raw images and masks are resized to 512x512 pixels for use in model training. A U-net model architecture is used based on previous success in identifying pixels corresponding to fascicles and aponeuroses (40,41). For both the superficial and deep aponeurosis models, the total image set is first randomized, then split into training (80% of the image set) and validation sets (20% of the image set). In this study, each model took approximately 1 hour to train (trainNetwork, Matlab) on a desktop computer with an Nvidia GTX 1660 Ti graphics card. From the validation set, pixel-wise mean classification accuracies were 96% and 94% and mean intersection over union values were 94% and 91% for the superficial and deep aponeuroses, respectively. The third step is applying the trained models to the broader dataset (~111,000 frames) and generation of first order polynomials to represent the superficial and deep aponeuroses which defines the region of interest for fascicle detection. This is accomplished by generating masks of both the superficial and deep aponeuroses from each frame of ultrasound data using the trained models (semanticseg, Matlab), identifying the largest object by area in each of the predicted masks, and then fitting a first order polynomial based on the centroid and orientation of each identified object (regionprops, Matlab). The intersection points of these superficial and deep first order polynomials with the proximal and distal borders of the image serve as the vertices bounding the region of interest. These regions of interest are then used in Part 2.

Part 2 – Representative Fascicle Estimation

A GUI-based Matlab application was developed to allow for streamlined visualization of representative fascicle measurements and correction of aponeurosis fits. The functionality of this

bioRxiv preprint doi: https://doi.org/10.1101/2025.08.20.671067; this version posted August 25, 2025. The copyright holder for this preprint (which was not certified by peer review) is the author/funder, who has granted bioRxiv a license to display the preprint in perpetuity. It is made available under a CC-BY 4.0 International license.

application is separated into 4 steps. First, the raw images, with fascicles running from top left to bottom right, are filtered using adaptive histogram equalization (adapthisteq, Matlab) to improve contrast of hyperechoic structures. To account for angled images, the user is prompted to enter the image angle, which is used to first shear the image to have vertical edges, then applies adaptive histogram equalization (adapthisteq, Matlab), then returns the image to the original angle. This step is necessary as the border outside an angled image introduces artifacts during filtering. From the filtered image, the area between the aponeuroses is identified as the region of interest, with all structures outside of that area being removed. The region of interest is binarized (imbinarize, Matlab) using a Frangi-type vessel enhancement filter (fibermetric, Matlab; thickness = 7, sensitivity = 100) as has been used in previous tracking algorithms (18,42,43). From this binarized image, the orientations and major axis lengths of each separate structure are computed (regionprops, Matlab). The user also has the option of further limiting the region of the image passed through to fascicle detection by applying an additional manual mask to these results, which may be warranted if the muscle of interest has compartments of different architectures. The second step is identification of the "snippets" in the binarized image which can be attributed to fascicles. Similar to (17), only structures with major axis lengths greater than 4 mm, area to length ratios less than 12, and with orientations relative to the deep aponeurosis within specified bounds are used to estimate the representative fascicle of each frame. The range of acceptable pennation angles relative to the deep aponeurosis was set between 6 and 20 degrees, based on *in-vivo* and cadaveric measurements of RF architecture (44,45) . The third step is assessment of the thickness of the muscle. This is calculated as the length of a line segment running perpendicular to the deep aponeurosis which intersects both the superficial aponeurosis and the midpoint of the deep aponeurosis. The fourth step is calculating representative fascicle parameters. The representative pennation angle of a frame is calculated as the circular mean weighted by snippet length from all accepted snippets, as adapted from (17). The representative fascicle length is then calculated as the thickness divided by the sine of this representative pennation angle (18,43,44). Following completed processing of a trial, the ensemble averaged and time normalized fascicle lengths and pennation angles are visualized. The application interface during use is included as a supplement (Figure S2). For all subsequent analyses, fascicle lengths and pennation angles were low-pass filtered at 6 Hz with a zero-phase 4^{th} order Butterworth filter. Fascicle velocities were calculated as the time derivative of filtered fascicle lengths.

bioRxiv preprint doi: https://doi.org/10.1101/2025.08.20.671067; this version posted August 25, 2025. The copyright holder for this preprint (which was not certified by peer review) is the author/funder, who has granted bioRxiv a license to display the preprint in perpetuity. It is made available under a CC-BY 4.0 International license.

Estimation of Fascicle and Muscle-Tendon Unit Energetics

Fascicle force was estimated from a Hill-type model of muscle force generation driven by a combination of experimentally measured fascicle lengths and muscle activations similar to (19):

$$F_{fas} = F_{max}[\hat{a}(t)\hat{F}_a(\hat{l}_{fas})\hat{F}_a(\hat{v}_{fas}) + \hat{F}_p(\hat{l}_{fas})] \quad \text{Eq 1}$$

Where F_{max} was maximum isometric fascicle force, $\hat{a}(t)$ was estimated muscle activation from EMG, $\hat{F}_a(\hat{l}_{fas})$ was the normalized relationship between active force and fascicle length, $\hat{F}_a(\hat{v}_{fas})$ was the normalized relationship between active force and fascicle velocity, and $\hat{F}_p(\hat{l}_{fas})$ was the relationship between passive force and normalized fascicle length. $\hat{l}_{fas}$ and $\hat{v}_{fas}$ were fascicle length and velocity, respectively, normalized to fascicle slack length, $l_{0,fas}$ (mean [s.d.]: 145.5 [22.4] mm across all participants). $l_{0,fas}$ was determined as the length when force began to appear in the tendon, which based on previous measurements of patellar tendon force in humans (46) was approximated for each participant to be the average fascicle length at 50% of the walking gait cycle at 1.25 m s^{-1}. MTU force was calculated as:

$$F_{MTU} = F_{fas} \cdot \cos(\alpha(t)) \quad \text{Eq 2}$$

Where $\alpha(t)$ is pennation angle. Maximum fascicle force was calculated as:

$$F_{max} = (\frac{V_m}{l_{fas,opt}})\sigma_0 \quad \text{Eq 3}$$

Where V_m is muscle volume estimated from each participants height and mass (47), σ_0 is specific muscle stress (48,49), and $l_{fas,opt}$ is optimal RF fiber length estimated from scaled OpenSim models of each participant (50). From (51,52), the normalized active force-length relationship was calculated as:

$$\hat{F}_a(\hat{l}_{fas}) = e^{-\left(\frac{\hat{l}_{fas}^{0.6}-1}{0.3}\right)^{2.3}} \quad \text{Eq 4}$$

For normalized fascicle lengths greater than unity, the normalized passive force-length relationship (53) was calculated as:

$$\hat{F}_p(\hat{l}_{fas}) = 2.64\hat{l}_{fas}^{\ 2} - 5.30\hat{l}_{fas} + 2.66 \quad \text{Eq 5}$$

For normalized fascicle lengths less than or equal to unity, the normalized passive force was set to 0. For shortening fascicles ($\hat{v}_{fas} \leq 0$), the normalized force-velocity relationship was given by (52):

bioRxiv preprint doi: https://doi.org/10.1101/2025.08.20.671067; this version posted August 25, 2025. The copyright holder for this preprint (which was not certified by peer review) is the author/funder, who has granted bioRxiv a license to display the preprint in perpetuity. It is made available under a CC-BY 4.0 International license.

$$\hat{F}_a(\hat{v}_{fas}) = \frac{1+\left(\frac{\hat{v}_{fas}}{\hat{v}_0}\right)}{1-\left(\frac{\hat{v}_{fas}}{\hat{v}_0\beta}\right)} \quad \text{Eq 6}$$

For lengthening fascicles ($\hat{v}_{fas}$ >0), the normalized force-velocity relationship was given by:

$$\hat{F}_a(\hat{v}_{fas}) = 1.5 - 0.5\frac{1-\left(\frac{\hat{v}_{fas}}{\hat{v}_0}\right)}{1+\left(\frac{7.56\cdot\hat{v}_{fas}}{\hat{v}_0\beta}\right)} \quad \text{Eq 7}$$

Where β was the fiber type dependent curvature of the force-velocity relationship (52). Since the human RF is of a mixed fiber type (38), β was determined to be the average of the constants determined from literature of both slow and fast fiber types (0.18 and 0.29, respectively; (19)). Similarly, $\hat{v}_0$, the maximum intrinsic speed of the fascicles, was estimated as the average (7.5 s^{-1}) of values from slow and fast fibers (5 and 10 s^{-1}, respectively (54,55)).

Since EMG and ultrasound images were collected from different legs, for all fascicle or MTU force, power, and work calculations information from both legs was combined. This was achieved by ensemble averaging activations, fascicle length/velocities, and MTU lengths/velocities, and fascicle pennation angles across all iterations of a given perturbation timing and side within each participant. Thus, within-participant and within-condition ensemble averaged timeseries were calculated for each stride (*e.g.*, one trace for all RF activations ipsilateral to the perturbed leg for participant 1 during early stance perturbations). Using these combined traces, fascicle power was calculated as the product of fascicle force and fascicle velocity, and MTU power was calculated as the product of MTU force and MTU velocity, where fascicle or MTU lengthening resulted in negative power, respectively. See Figure 2C for an overview of fascicle and MTU force and power calculations. Fascicle and MTU work values were calculated by integrating the ensemble averaged curves (trapz, Matlab) and then multiplying by the average stride duration of the traces divided by the number of normalized time points of each stride (101). To compare leg or joint level mechanical work values with fascicle and MTU mechanical work, mechanical work at the leg or joint levels was also averaged across all perturbation iterations within each participant.

bioRxiv preprint doi: https://doi.org/10.1101/2025.08.20.671067; this version posted August 25, 2025. The copyright holder for this preprint (which was not certified by peer review) is the author/funder, who has granted bioRxiv a license to display the preprint in perpetuity. It is made available under a CC-BY 4.0 International license.

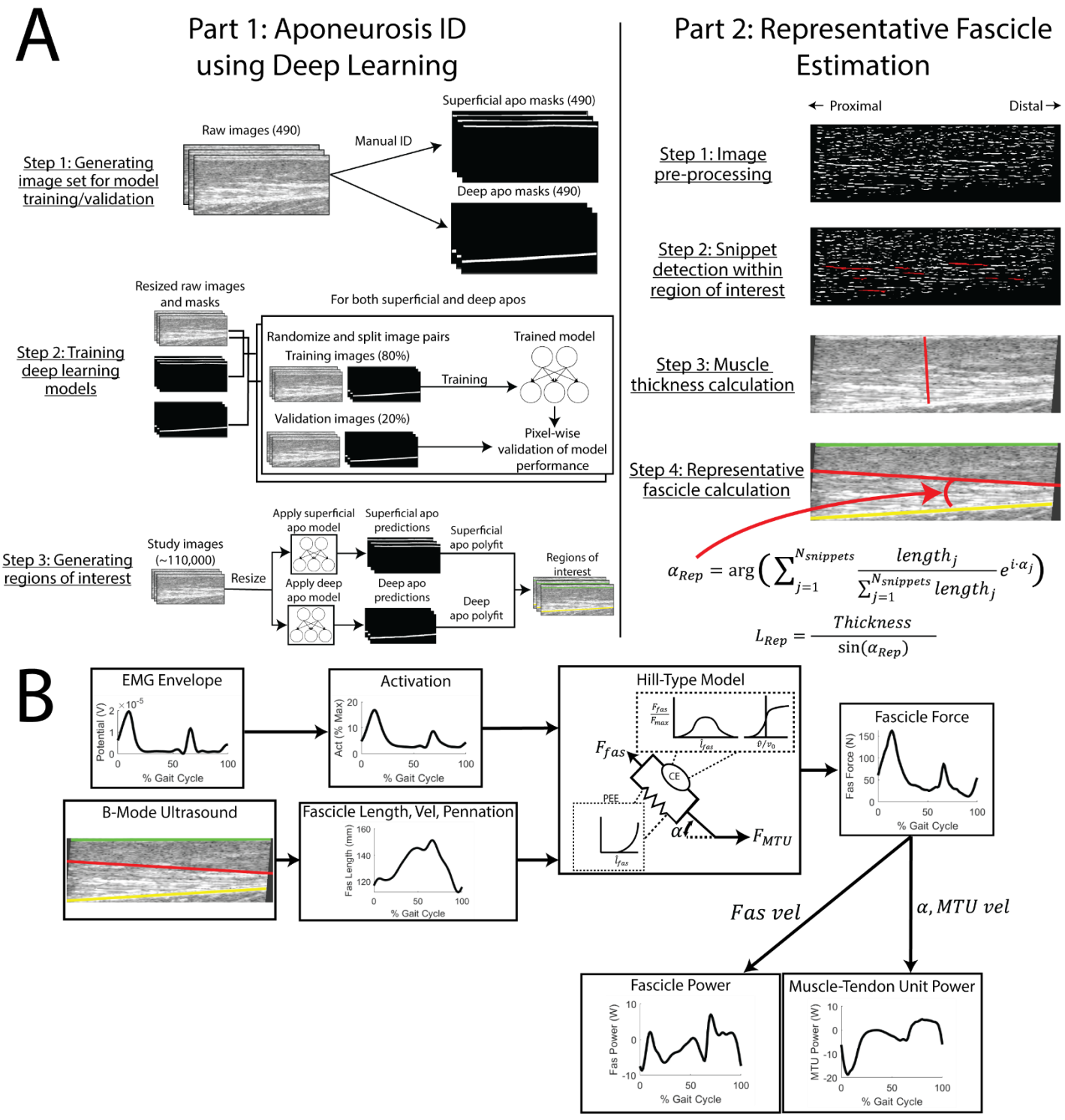


Figure 2 – A) Overview of custom fascicle tracker application. α = fascicle pennation angle, L_{Rep} = representative fascicle length. B) Overview of fascicle and muscle-tendon unit energetics computation. CE = contractile element, PEE = passive elastic element.

bioRxiv preprint doi: https://doi.org/10.1101/2025.08.20.671067; this version posted August 25, 2025. The copyright holder for this preprint (which was not certified by peer review) is the author/funder, who has granted bioRxiv a license to display the preprint in perpetuity. It is made available under a CC-BY 4.0 International license.

Statistical Analysis

Statistical analyses were performed in Matlab R2019b (Mathworks, Natick, MA, USA). To investigate differences in timeseries outcomes (e.g., fascicle lengths, activations, mechanical powers for H1), statistical parametric mapping (SPM; (56)) was used to run paired t-tests to compare early or late stance traces to steady state traces (*i.e.*, the pre-perturbation stride) without needing to correct for multiple comparisons. While all statistical differences were reported, alterations in stride times due to the perturbations led to phase shifts in the gait-cycle normalized data that resulted in some periods of statistical significance that were not determined to be meaningful. Further, p-values greater than the significance threshold (*i.e.*, 0.05) were approximated by solving p-value associated with the maximum t-statistic during the entire timeseries. This approach has not yet been validated (57) and in some cases resulted in values less than the significance threshold. Such cases are denoted with *ns*. All timeseries data were represented in relation to the gait cycle of the perturbed (i.e., ipsilateral) leg. For discrete outcome measures such as mechanical work, paired t-tests were used to compare early or late stance perturbation conditions to steady state levels (H2 and H3). To evaluate the functional role of the RF in relation to the hip, knee, and overall leg (H2), linear regressions were used to relate changes in fascicle or MTU work to changes in hip, knee, and overall leg work relative to steady state levels (i.e., the work of the perturbed stride – work of the previous unperturbed stride, S-1). Since the hip had 3 degrees of freedom in these analyses, hip work was calculated as the integrated sum of all 3 components to better account for overall leg work. Analyses were limited to the unperturbed, perturbed (S0), and first recovery strides (S+1) as a return to steady state in external kinetics and kinematics was largely achieved after the first recovery stride (8). Because data were collapsed across perturbation iterations, for each leg these regressions contained 14 points (7 participants x 2 timings) instead of 222 from all perturbations. Significance was concluded for p-values ≤ 0.05.

Results

During perturbations, rectus femoris fascicle rotation decouples length changes between MTU and fascicles levels, with increased activation driving active lengthening.

For both early and late stance perturbations, during the perturbed stride (S0) on the ipsilateral leg there was no significant length change of RF fascicles (early: $p = 0.679$; late: $p = 0.078$), while there was significant lengthening of the MTU (early: $p < 0.001$; late: $p = 0.022$; Figure 3). This decoupling during perturbations appeared to be caused by increases in pennation angle (early: $p = 0.080$; late: $p = 0.180$) offsetting increases in muscle thickness (early: $p = 0.201$; late: $p=0.033$ *ns;* Figure 3). Further,

bioRxiv preprint doi: https://doi.org/10.1101/2025.08.20.671067; this version posted August 25, 2025. The copyright holder for this preprint (which was not certified by peer review) is the author/funder, who has granted bioRxiv a license to display the preprint in perpetuity. It is made available under a CC-BY 4.0 International license.

although not statistically significant, an increase in RF activation relative to steady state levels was also observed (early: $p = 0.080$; late: $p = 0.036$ *ns*; Figure 4). The natural lengthening of RF fascicles from mid to late stance coupled with increased activation resulted in increased fascicle forces during mid to late stance for early stance perturbations and around toe-off for late stance perturbations ($p<0.001$ for both; Figure 4). This increased force during lengthening resulted in larger negative powers and work at the level of the RF fascicles and the MTU (Figure 5). At the level of fascicles, negative powers during stance were not significantly different from steady state for either timing (early: $p = 0.025$ *ns*; late: $p= 0.475$), while significantly more negative work was performed over the perturbed stride for both timings (early: $p < 0.001$; late: $p = 0.039$). At the level of the MTU, there were significantly larger negative power relative to steady state for both timings ($p < 0.001$ for both), which also resulted in significantly more negative work (early: $p = 0.002$; late: $p = 0.003$).

Rectus femoris mechanical energetics on the contralateral leg and first recovery stride

On the contralateral leg to the perturbation, during the perturbed stride (S0), early stance perturbations were associated with longer fascicle and MTU lengths relative to steady state, followed by shortening ($p < 0.001$) to allow lengths to return to steady state levels around contralateral heelstrike (Figure 3). This shortening coincided with increased RF activation ($p = 0.025$ *ns*) to result in increased forces ($p < 0.001$; Figure 4) and larger positive fascicle and MTU powers ($p < 0.001$; Figure 5). However, for fascicles, these larger positive powers were offset by larger negative powers later in the gait cycle which resulted in fascicles performing larger amounts of negative work over the perturbed stride relative to steady state ($p < 0.001$; Figure 5). Conversely, for the MTU, the larger negative power during the perturbation was not fully offset and the net work performed by the MTU was greater than steady state levels, though this difference was not significant ($p = 0.076$; Figure 5).

For late stance perturbations, changes from steady state were predominantly limited to increased activations ($p < 0.001$) and forces ($p < 0.001$) coinciding with steady state levels of fascicle and MTU lengthening. This resulted in larger negative fascicle ($p = 0.018$) and MTU works ($p = 0.002$) relative to steady state.

Across both legs, the largest deviations from steady state on the first recovery stride (S+1) occurred following late stance perturbations on the contralateral side. While contralateral MTU lengths were shorter relative to steady state ($p < 0.001$), the contralateral RF fascicles lengthened then shortened during swing, although not significantly ($p = 0.082$), due to increasing pennation offsetting

bioRxiv preprint doi: https://doi.org/10.1101/2025.08.20.671067; this version posted August 25, 2025. The copyright holder for this preprint (which was not certified by peer review) is the author/funder, who has granted bioRxiv a license to display the preprint in perpetuity. It is made available under a CC-BY 4.0 International license.

increased thickness ($p < 0.001$; Figure 3). Increased RF activations drove higher forces ($p < 0.001$; Figure 4), which resulted in a period of negative followed by positive fascicle power, which on net over the first recovery stride led to slightly more negative work being performed by the fascicles relative to steady state ($p = 0.018$; Figure 5). In general, changes in both ipsilateral and contralateral fascicle and MTU work from steady state levels were minimal during the first recovery stride.

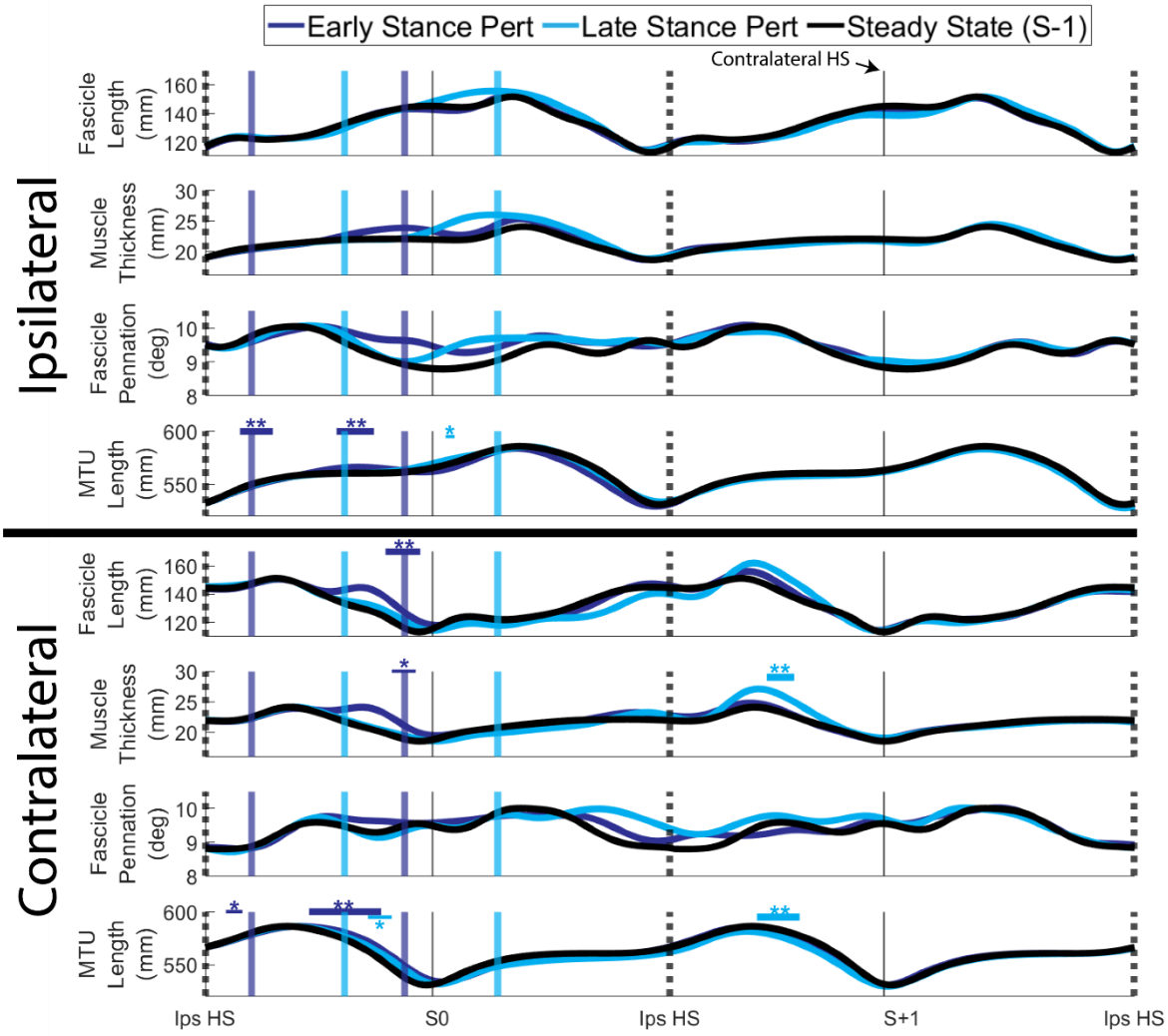


Figure 3 – Rectus femoris fascicle and MTU dynamics on both legs relative to the perturbation across all participants (n=7, 222 perturbations), time-normalized to gait cycles. Standard deviations were omitted for clarity. Instances when curves significantly deviated from steady state (S-1) as determined by statistical parametric mapping two-tailed t-tests are identified with thick horizontal lines and ** for $p < 0.001$, and thin horizontal lines and * for $p < 0.05$. Solid colored vertical lines indicate average start and end times of the perturbations. Dotted/solid black vertical lines indicate instances of ipsilateral/contralateral heelstrike, respectively. "Steady State" strides were the strides preceding the perturbed stride (S-1).

bioRxiv preprint doi: https://doi.org/10.1101/2025.08.20.671067; this version posted August 25, 2025. The copyright holder for this preprint (which was not certified by peer review) is the author/funder, who has granted bioRxiv a license to display the preprint in perpetuity. It is made available under a CC-BY 4.0 International license.

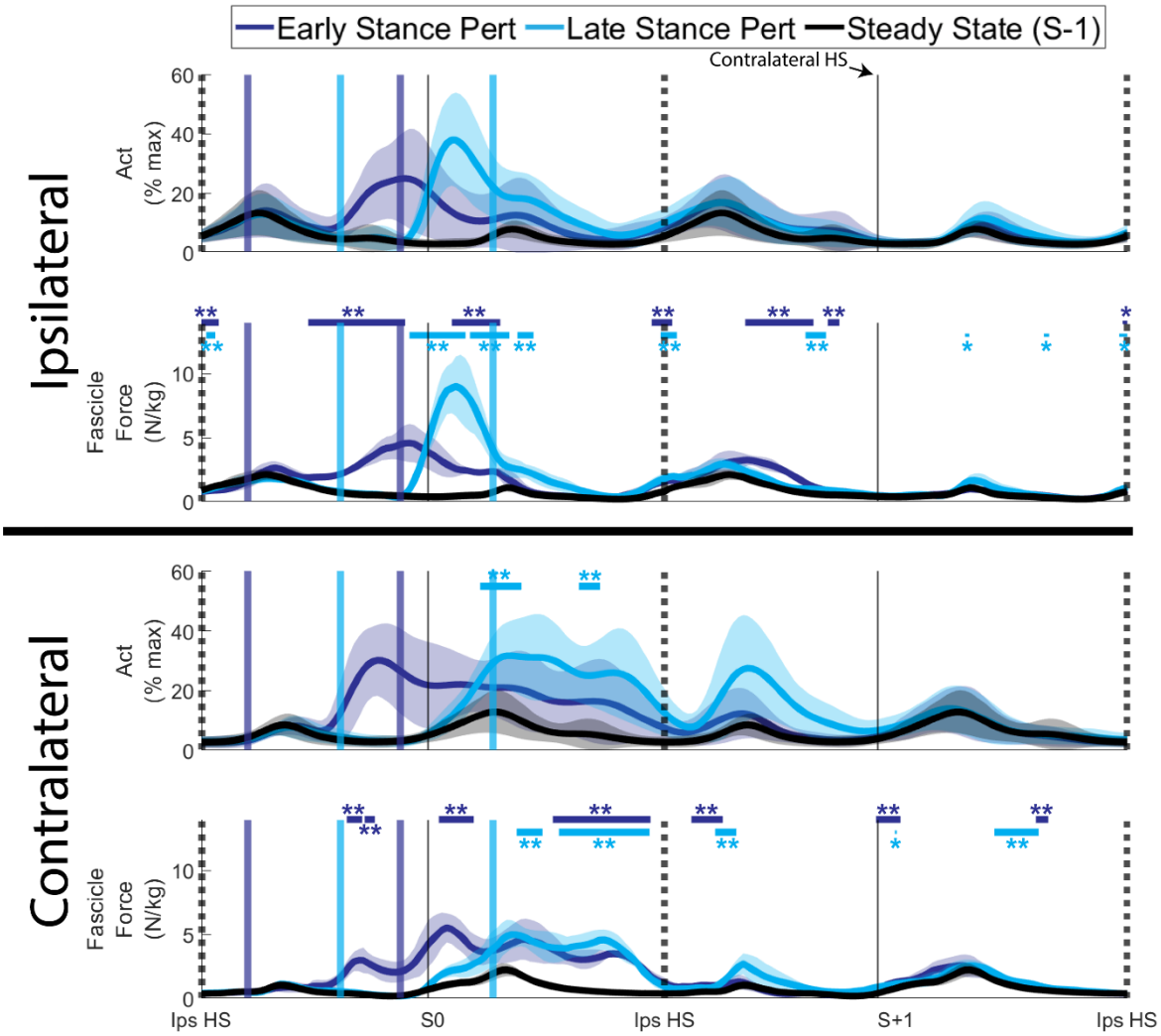


Figure 4 – Rectus femoris activations (% max across all trials) and fascicle forces on both legs relative to the perturbation across all participants (n=7, 222 perturbations), time-normalized to gait cycles. Shaded regions represent ±1 standard deviation. Instances when curves significantly deviated from steady state (S-1) as determined by statistical parametric mapping two-tailed t-tests are identified with thick horizontal lines and ** for p < 0.001, and thin horizontal lines and * for p < 0.05. Solid colored vertical lines indicate average start and end times of the perturbations. Dotted/solid black vertical lines indicate instances of ipsilateral/contralateral heelstrike, respectively. "Steady State" strides were the strides preceding the perturbed stride (S-1).

bioRxiv preprint doi: https://doi.org/10.1101/2025.08.20.671067; this version posted August 25, 2025. The copyright holder for this preprint (which was not certified by peer review) is the author/funder, who has granted bioRxiv a license to display the preprint in perpetuity. It is made available under a CC-BY 4.0 International license.

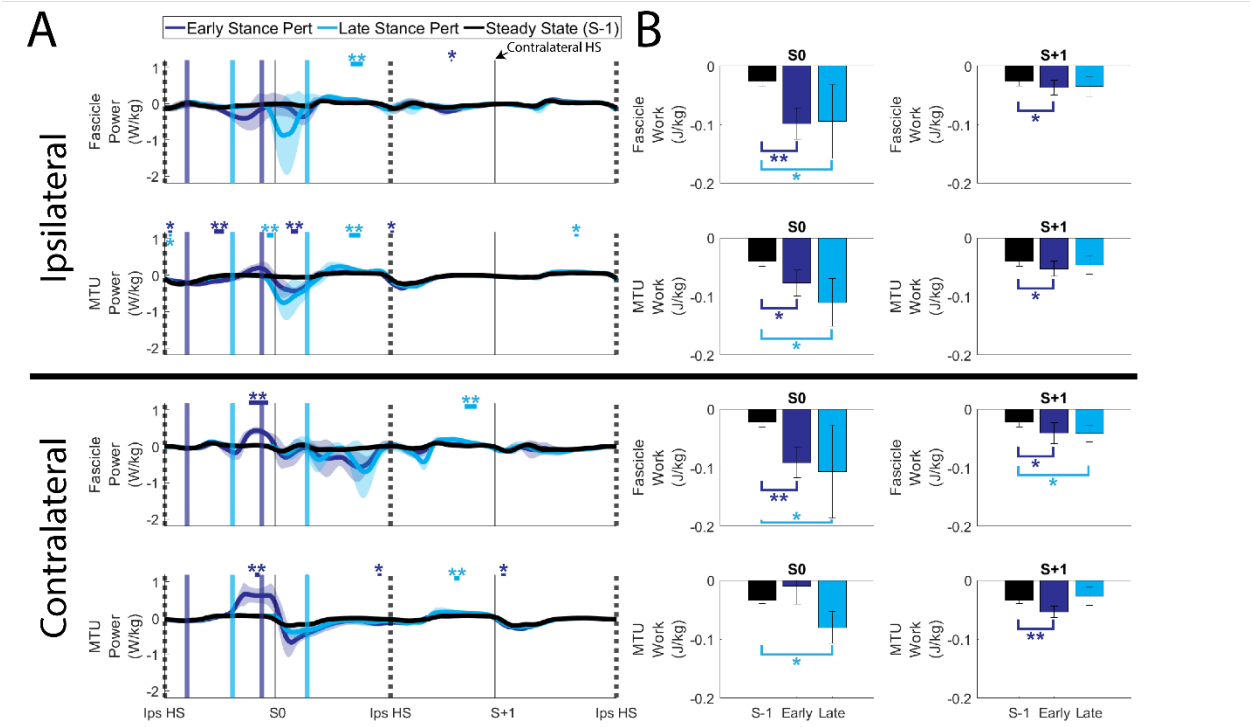


Figure 5 - A) Rectus femoris fascicle and MTU mechanical powers on both legs relative to the perturbation across all participants (n=7, 222 perturbations), time-normalized to gait cycles. Shaded regions represent ±1 standard deviation. Instances when curves significantly deviated from steady state (S-1) as determined by statistical parametric mapping two-tailed t-tests are identified with thick horizontal lines and ** for p < 0.001, and thin horizontal lines and * for p < 0.05. Solid colored vertical lines indicate average start and end times of the perturbations. Dotted/solid black vertical lines indicate instances of ipsilateral/contralateral heelstrike, respectively. "Steady State" strides were the strides preceding the perturbed stride (S-1). B) Rectus femoris fascicle and MTU work over the perturbed (S0) and first recovery stride (S+1) on both sides relative to the perturbation. Within-participant paired two-tailed t-test results comparing perturbed to steady state (S-1) values are represented as ** for p<0.001 and * for p<0.05.

The rectus femoris MTU best reflects the role of the contralateral hip

Changes in RF MTU work most strongly related to changes in hip work on the leg contralateral to the perturbation during both the perturbed and first recovery strides. Fascicles had much weaker relationships to joint level demands compared to MTUs (max R^2 = 0.22, p > 0.051), although the direction of the relationships was general consistent across fascicle and MTU levels for a given leg and stride (Figure 6). Further, relationships between both fascicle and MTU levels with leg level demands were consistently weak (max R^2 across all = 0.22, p > 0.051)

bioRxiv preprint doi: https://doi.org/10.1101/2025.08.20.671067; this version posted August 25, 2025. The copyright holder for this preprint (which was not certified by peer review) is the author/funder, who has granted bioRxiv a license to display the preprint in perpetuity. It is made available under a CC-BY 4.0 International license.

On the perturbed stride (S0), contrary to our hypothesis, the RF MTU had the strongest positive relationship with the hip (MTU R^2 = 0.74, $p < 0.001$) and a weaker negative relationship with the knee (MTU R^2 = 0.48, p = 0.004). On the first recovery stride (S+1), there was also a strong positive relationship between RF MTU and hip demands (R^2 = 0.52, p = 0.002).

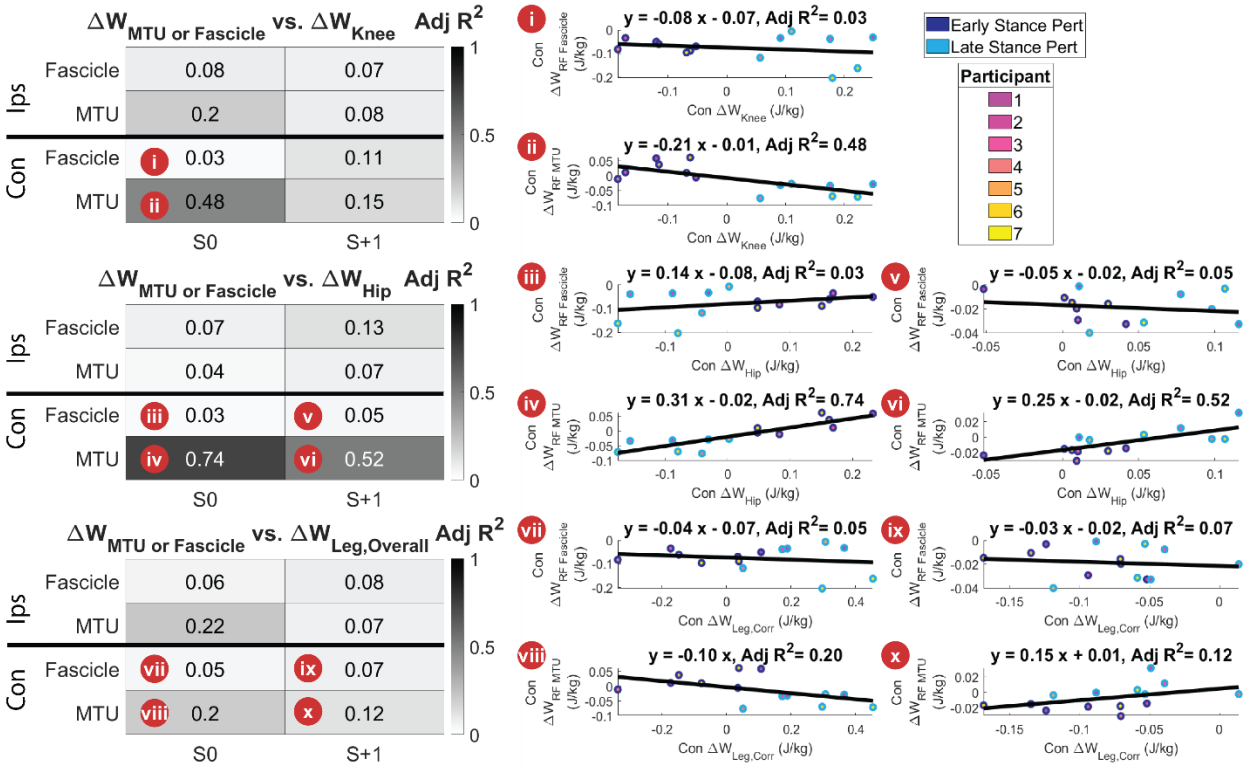


Figure 6 – Relationships between rectus femoris fascicle or MTU work and the knee, hip, and overall leg. Heatmaps show adjusted R^2 values for linear regressions between differences in fascicle or MTU work over a stride from steady state, and differences in knee, hip, or corrected leg work over a stride from steady state (S-1). Note that fascicle and MTU data were collapsed across iterations and sides, resulting in 14 data points (n=7, 2 perturbation timings) per scatter from the original 222 perturbations. (i-x) Scatter plots for selected fascicle and MTU relationships of interest.

Discussion

The main objective of this work was to evaluate the role of the RF in mediating transient mechanical energy demands during perturbed walking in humans. Using unilateral belt accelerations on a split-belt treadmill, we imposed quantifiable mechanical energy demands on both legs during walking and extended our previous analysis relating joint and leg level demands down to the level of the RF MTU and fascicles (8). To estimate mechanical power and work of the RF for this approach, we used *in-vivo* RF fascicle lengths measured using B-mode ultrasound and a custom fascicle tracking application in conjunction with EMG to drive a Hill-type model of force generation. Our first hypothesis (H1) sought to

bioRxiv preprint doi: https://doi.org/10.1101/2025.08.20.671067; this version posted August 25, 2025. The copyright holder for this preprint (which was not certified by peer review) is the author/funder, who has granted bioRxiv a license to display the preprint in perpetuity. It is made available under a CC-BY 4.0 International license.

address the energetic implications of the perturbation itself – specifically, we hypothesized that on the perturbed leg, the perturbation would result in negative RF power and work because of active muscle lengthening. Our results partially supported this first hypothesis, with the kinematics of the perturbation resulting in lengthening of the RF MTU relative to steady state walking, but not the RF fascicles. This decoupling was due to an increase in fascicle pennation angle offsetting a potential increase in fascicle length due to increased muscle thickness. While decoupling during eccentric contractions due to changes in architectural gearing have previously been observed, such changes are due to a decrease in thickness being offset by a decrease in pennation angle. This discrepancy is likely due to changes in slope of the deep aponeurosis – during perturbations we observed that the deep aponeurosis exhibited an increased slope relative to steady state, thereby increasing the measured thickness and increasing the measured pennation angle (Figure S3). Linear regressions between deep aponeurosis angle and pennation angle (R^2=0.37, p<0.001) in addition to the sine of deep aponeurosis angle and thickness (R^2=0.14, p<0.001) over the stance phase on the perturbed leg further support this relationship. However, our hypothesis was still partially supported since increased RF activation during the perturbation together with similar lengthening observed during steady state walking precipitated increased negative power and work. While this represents the first *in-vivo* estimate of rectus femoris mechanical energetics during perturbed walking, the dissipation induced by the perturbation at proximal MTU and fascicle levels is mechanically analogous to other transient, dissipation-inducing perturbations delivered at distal sites. Specifically, unexpected changes in substrate height have been extensively investigated in both hopping humans and running guinea fowl (5–7), with drops in ground height resulting in active lengthening of the plantarflexors. In perturbed human hopping, a drop in terrain height has been shown to extend the aerial phase and thus shift the onset timing of plantarflexor activation to be earlier relative to ground contact. This earlier activation in concert with coactivation of the tibialis anterior has been demonstrated to: 1) allow plantarflexor muscles to pre-emptively shorten before ground contact, allowing for lower, potentially less damaging muscle strains, 2) stiffen and stabilize the ankle, and 3) bias the muscle towards achieving the task demand (*i.e.*, dissipation of injected energy) due to alignment of activation and fascicle lengthening (7,58). We now address each of those previous findings in light of our results. In our perturbation context, instead of delaying the onset of ground contact, we applied both perturbation timings within stance phase, which did not allow for a pre-emptive shortening during an unloaded period. However, even without this pre-emptive shortening, we observed steady-state magnitudes of fascicle lengthening during the perturbations. While buffering of length changes between the MTU and fascicle levels in other quadriceps muscles has previously been

bioRxiv preprint doi: https://doi.org/10.1101/2025.08.20.671067; this version posted August 25, 2025. The copyright holder for this preprint (which was not certified by peer review) is the author/funder, who has granted bioRxiv a license to display the preprint in perpetuity. It is made available under a CC-BY 4.0 International license.

attributed to series elasticity (59), we found that such lengthening may be buffered by shape change of the deep aponeurosis. Consistent with previous work investigating changes in activation of leg musculature during walking on uneven terrain (60), we observed coactivation of muscles across the lower limb on the perturbed leg (Figure S1), with increases in plantarflexor activation occurring first and being the most prominent. However, a previous study specifically investigating unilateral treadmill belt accelerations did not see increases in tibialis anterior activity following plantarflexor activation, which could be attributed to the less intense perturbations not eliciting a whole-leg coactivation strategy (61). Lastly, on the perturbed leg, we previously found the overall leg level demand of early stance perturbations was generation of net work over a stride, and the demand of late stance perturbations was net zero work over a stride, since net positive work performed by the leg on the treadmill is offset by net negative work performed by the leg on the COM (8). Therefore, in contrast to tasks where plantarflexors have been shown to modulate their mechanical role to match that of the limb (5–7), during a treadmill acceleration task the RF on the perturbed leg predominantly serves to dissipate energy and thus does not directly represent the energetic role of the leg, knee, or hip (Figure 6).

Despite the RF not reflecting the role of joints or the leg on the perturbed side, since we previously identified the contralateral knee as reflecting the energetic demand on the contralateral leg, we hypothesized due to the similar “damping” functions of the knee and RF (H2) that the contralateral RF may reflect knee, and therefore leg level demands on the perturbed stride. In contrast to our hypothesis, the RF, particularly at the MTU (vs. fascicle) level, best reflected the role of the contralateral hip, while the relationship between the RF and the knee and leg were weaker and negative (Figure 6). This relationship was due to 1) early stance perturbations eliciting positive net work at the hip joint and the MTU and fascicles actively shortening during swing to produce a period of positive power and 2) late stance perturbations eliciting negative work at the hip joint and the MTU and fascicles actively lengthening during stance to produce almost exclusively negative power. In contrast, the work demands on the knee are opposite to that of the hip during these perturbation timings (*i.e.*, net negative knee work during early stance perturbations, net positive knee work during late stance perturbations). These findings indicate that while the role of the RF during unperturbed walking is generally dissipation of mechanical energy (24) and this role can amplified or attenuated depending on the timing of the perturbation.

When interpreting our findings, two important technical limitations should be considered. The first limitation is that RF fascicle lengths measured using the custom tracking application were not

bioRxiv preprint doi: https://doi.org/10.1101/2025.08.20.671067; this version posted August 25, 2025. The copyright holder for this preprint (which was not certified by peer review) is the author/funder, who has granted bioRxiv a license to display the preprint in perpetuity. It is made available under a CC-BY 4.0 International license.

validated against gold-standard measurement tools such as diffusion tensor imaging or extended field of view techniques (62,63). Further, comparison against hand-tracked ultrasound images may not serve as a high-fidelity standard because 2D ultrasound images cannot capture the complex 3D shape changes of the muscle (64), high frame rate ultrasound imaging still necessitates the extrapolation of fascicle lengths from the imaged section of the muscle, and manual tracking of a single fascicle would likely have more variability than tracking all fascicles within the imaged section of the RF. We are confident in our tracking application because 1) the selection of snippets used to calculate a representative fascicle was similar to that of a previously validated application (17), 2) only snippets within a physiological range of pennation angles were used to estimate a representative fascicle, 3) the thickness of the muscle was calculated from hand-tracked aponeuroses for each frame, 4) for within-subject designs, our extrapolation method has been shown to be acceptable for estimating normalized fascicle lengths of other quadriceps muscles (65). Further, the range of RF fascicle strains we observed during unperturbed walking (0.8 to 1.08 of fascicle slack length) are more physiologically plausible than the range reported from simulated RF fiber length during walking at 1.25 m s^{-1} (0.7 to 1.4 of optimal fiber length; (34)), when considering active strains above 25% being potentially damaging (66). The second important limitation is that we estimated fascicle and MTU forces using a Hill-type model, which is known to have shortcomings when predicting *in-vivo* forces and energetics (19,54,55,67–69). Multiple aspects of Hill-type models have been suggested to contribute to these discrepancies, a subset of which are: 1) that Hill-type models are based on phenomenological relationships characterized at maximal activations, which may explain inaccuracies when estimating forces at physiological, submaximal levels (19,54,67), 2) classical Hill-type models have independent length, velocity, and activation components and thus do not capture physiological relationships between length and activation (70–72) or velocity and activation (73), and 3) Hill-type models do not capture the history dependence of muscle force, which may play an important role in responses to perturbations (74–76). Despite these shortcomings, the computational tractability of Hill-type models has resulted in them becoming the state of the art for use in simulations of human movement (34,77,78). By using *in-vivo* estimates of fascicle length and activation to drive a Hill-type model, our approach represents a potential improvement over other fully computational approaches by avoiding assumptions about force sharing among quadriceps muscles and the influence of series elasticity from aponeuroses and the external tendon, both of which are particularly relevant for the RF (79,80).

To conclude, this study extended a previous investigation of the relationship between joint and leg level mechanical energetics during perturbed walking down to the level of the RF MTU and fascicles.

bioRxiv preprint doi: https://doi.org/10.1101/2025.08.20.671067; this version posted August 25, 2025. The copyright holder for this preprint (which was not certified by peer review) is the author/funder, who has granted bioRxiv a license to display the preprint in perpetuity. It is made available under a CC-BY 4.0 International license.

This was accomplished by coupling in-vivo EMG and B-mode ultrasound imaging in conjunction with a Hill-type model of muscle force. We found that on the perturbed leg the RF MTU and fascicles actively lengthened during perturbations, but fascicle lengthening was limited due to shape change of the deep aponeurosis, 2) on the contralateral side the RF, particularly at the MTU level, better reflected energetic demands on the hip as opposed to the knee and leg levels, and 3) on the perturbed leg the RF acted to shuttle energy across the leg to fulfill the overall leg-level demand. We anticipate future work will use such multi-scale approaches to better understand how changes in muscle-level dynamics explain altered joint and leg level demands during use of assistive devices (36), and following injury (81). Further, muscle-level measurements coupled with models of physiological sensory organs can provide a window into the signals and motor programs used by the nervous system to maintain stability during locomotion (82–84).

1.1 Ethics

All participants (recruitment period: 8/28/2020 - 3/6/2021) provided written informed consent and all protocols were approved by the Institutional Review Board at the Georgia Institute of Technology (Protocol H20163).

1.2 Data Accessibility

The ultrasound processing scripts are available at https://github.com/pgolyski/RF_US_DL and biomechanical data for all participants (N=7) are available at: https://zenodo.org/doi/10.5281/zenodo.12728475

1.3 Authors' Contributions

Pawel R. Golyski: Conceptualization, Data curation, Formal analysis, Methodology, Visualization, Writing – original draft, Writing – review & editing.

Gregory S. Sawicki: Conceptualization, Funding acquisition, Writing – review & editing, Project administration, Supervision

1.4 Competing Interests

The authors have declared that no competing interests exist.

bioRxiv preprint doi: https://doi.org/10.1101/2025.08.20.671067; this version posted August 25, 2025. The copyright holder for this preprint (which was not certified by peer review) is the author/funder, who has granted bioRxiv a license to display the preprint in perpetuity. It is made available under a CC-BY 4.0 International license.

1.5 Funding

This research was supported by the U.S. Army Natick Soldier Research, Development, and Engineering Center (W911QY18C0140) to Gregory S. Sawicki and the National Science Foundation (DGE-1650044) to Pawel R. Golyski.

1.6 Acknowledgements

The authors thank Jennifer Leestma for her development of the perturbation program and insightful discussions, in addition to Patrick Kim and Nicholas Swaich for assistance with data collection.

bioRxiv preprint doi: https://doi.org/10.1101/2025.08.20.671067; this version posted August 25, 2025. The copyright holder for this preprint (which was not certified by peer review) is the author/funder, who has granted bioRxiv a license to display the preprint in perpetuity. It is made available under a CC-BY 4.0 International license.

References

1. Joshi V, Srinivasan M. A controller for walking derived from how humans recover from perturbations. J R Soc Interface. 2019 Aug 1;16(157).

2. Vlutters M, Van Asseldonk EHF, Van Der Kooij H. Center of mass velocity-based predictions in balance recovery following pelvis perturbations during human walking. Journal of Experimental Biology. 2016 May 15;219(10):1514–23.

3. Nakazawa K, Kawashima N, Akai M, Yano H. On the reflex coactivation of ankle flexor and extensor muscles induced by a sudden drop of support surface during walking in humans. J Appl Physiol. 2004;96:604–11.

4. Schillings AM, Van Wezel BMH, Mulder T, Duysens J. Muscular responses and movement strategies during stumbling over obstacles. J Neurophysiol. 2000;83(4):2093–102.

5. Daley MA, Voloshina A, Biewener AA. The role of intrinsic muscle mechanics in the neuromuscular control of stable running in the guinea fowl. Journal of Physiology. 2009;587(11):2693–707.

6. Daley MA, Biewener AA. Leg muscles that mediate stability: Mechanics and control of two distal extensor muscles during obstacle negotiation in the guinea fowl. Philosophical Transactions of the Royal Society B: Biological Sciences. 2011;366(1570):1580–91.

7. Dick TJM, Clemente CJ, Punith LK, Sawicki GS. Series elasticity facilitates safe plantar flexor muscle-tendon shock absorption during perturbed human hopping. Proceedings of the Royal Society B: Biological Sciences. 2021 Mar 31;288(1947).

8. Golyski PR, Sawicki GS. Which lower limb joints compensate for destabilizing energy during walking in humans? J R Soc Interface. 2022 Jun;19(191).

9. Sánchez N, Simha SN, Donelan JM, Finley JM. Taking advantage of external mechanical work to reduce metabolic cost: the mechanics and energetics of split-belt treadmill walking. Journal of Physiology. 2019;597(15):4053–68.

10. Selgrade BP, Thajchayapong M, Lee GE, Toney ME, Chang YH. Changes in mechanical work during neural adaptation to asymmetric locomotion. Journal of Experimental Biology. 2017;220(16):2993–3000.

11. Zelik KE, Takahashi KZ, Sawicki GS. Six degree-of-freedom analysis of hip, knee, ankle and foot provides updated understanding of biomechanical work during human walking. Journal of Experimental Biology. 2015;218(6):876–86.

12. Daley MA, Felix G, Biewener AA. Running stability is enhanced by a proximo-distal gradient in joint neuromechanical control. Journal of Experimental Biology. 2007;210(3):383–94.

13. Dick TJM, Punith LK, Sawicki GS. Humans falling in holes: Adaptations in lower-limb joint mechanics in response to a rapid change in substrate height during human hopping. J R Soc Interface. 2019;16(159).

bioRxiv preprint doi: https://doi.org/10.1101/2025.08.20.671067; this version posted August 25, 2025. The copyright holder for this preprint (which was not certified by peer review) is the author/funder, who has granted bioRxiv a license to display the preprint in perpetuity. It is made available under a CC-BY 4.0 International license.

14. Farris DJ, Raiteri BJ. Modulation of leg joint function to produce emulated acceleration during walking and running in humans. R Soc Open Sci. 2017 Mar 8;4(3).

15. Qiao M, Jindrich DL. Leg joint function during walking acceleration and deceleration. J Biomech. 2016;49(1):66–72.

16. Schache AG, Lai AKM, Brown NAT, Crossley KM, Pandy MG. Lower-limb joint mechanics during maximum acceleration sprinting. Journal of Experimental Biology. 2019;222(22).

17. Marzilger R, Legerlotz K, Panteli C, Bohm S, Arampatzis A. Reliability of a semi-automated algorithm for the vastus lateralis muscle architecture measurement based on ultrasound images. Eur J Appl Physiol [Internet]. 2018;118(2):291–301. Available from: http://dx.doi.org/10.1007/s00421-017-3769-8

18. van der Zee TJ, Kuo AD. TimTrack: A drift-free algorithm for estimating geometric muscle features from ultrasound images. PLoS One. 2022 Mar 24;17(3):e0265752.

19. Dick TJM, Biewener AA, Wakeling JM. Comparison of human gastrocnemius forces predicted by Hill-type muscle models and estimated from ultrasound images. Journal of Experimental Biology. 2017;220(9):1643–53.

20. Konow N, Roberts TJ. The series elastic shock absorber: Tendon elasticity modulates energy dissipation by muscle during burst deceleration. Proceedings of the Royal Society B: Biological Sciences. 2015;282(1804).

21. Debelle H, Harkness-Armstrong C, Hadwin K, Maganaris CN, O'Brien TD. Recovery From a Forward Falling Slip: Measurement of Dynamic Stability and Strength Requirements Using a Split-Belt Instrumented Treadmill. Front Sports Act Living. 2020;2(July):1–13.

22. Arampatzis A, De Monte G, Karamanidis K, Morey-Klapsing G, Stafilidis S, Brüggemann GP. Influence of the muscle-tendon unit's mechanical and morphological properties on running economy. Journal of Experimental Biology. 2006;209(17):3345–57.

23. Biewener AA, Roberts TJ. Muscle and tendon contributions to force, work, and elastic energy savings: a comparative perspective. Exerc Sport Sci Rev. 2000 Jul;28(3):99–107.

24. Lai AKM, Biewener AA, Wakeling JM. Muscle-specific indices to characterise the functional behaviour of human lower-limb muscles during locomotion. J Biomech [Internet]. 2019 May 24;89:134–8. Available from: http://www.ncbi.nlm.nih.gov/pubmed/31036379

25. Zeni JA, Higginson JS. Gait parameters and stride-to-stride variability during familiarization to walking on a split-belt treadmill. Clinical Biomechanics. 2010 May;25(4):383–6.

26. Golyski PR, Vazquez E, Leestma JK, Sawicki GS. Onset timing of treadmill belt perturbations influences stability during walking. J Biomech. 2021 Oct;110800.

27. Liu C, de Macedo L, Finley JM. Conservation of reactive stabilization strategies in the presence of step length asymmetries during walking. Front Hum Neurosci. 2018 Jun 27;12.

bioRxiv preprint doi: https://doi.org/10.1101/2025.08.20.671067; this version posted August 25, 2025. The copyright holder for this preprint (which was not certified by peer review) is the author/funder, who has granted bioRxiv a license to display the preprint in perpetuity. It is made available under a CC-BY 4.0 International license.

28. van den Bogert AJ, Geijtenbeek T, Even-Zohar O, Steenbrink F, Hardin EC. A real-time system for biomechanical analysis of human movement and muscle function. Med Biol Eng Comput. 2013 Oct;51(10):1069–77.

29. Rajagopal A, Dembia CL, DeMers MS, Delp DD, Hicks JL, Delp SL. Full-Body Musculoskeletal Model for Muscle-Driven Simulation of Human Gait. IEEE Trans Biomed Eng [Internet]. 2016 Oct;63(10):2068–79. Available from: file:///C:/Users/Carla%0ACarolina/Desktop/Artigos%0Apara%0Aacrescentar%0Ana%0Aqualificação/The%0Aimpact%0Aof%0Abirth%0Aweight%0Aon%0Acardiovascular%0Adisease%0Arisk%0Ain

30. Delp SL, Anderson FC, Arnold AS, Loan P, Habib A, John CT, et al. OpenSim: Open-source software to create and analyze dynamic simulations of movement. IEEE Trans Biomed Eng. 2007;54(11):1940–50.

31. Donelan JM, Kram R, Kuo AD. Simultaneous positive and negative external mechanical work in human walking. J Biomech. 2002;35(1):117–24.

32. Cavagna GA, Kaneko M. Mechanical work and efficiency in level walking and running. J Physiol. 1977 Jun 1;268(2):467–81.

33. Willems PA, Cavagna GA, Heglund NC. External, internal and total work in human locomotion. J Exp Biol. 1995 Feb;198(Pt 2):379–93.

34. Arnold EM, Hamner SR, Seth A, Millard M, Delp SL. How muscle fiber lengths and velocities affect muscle force generation as humans walk and run at different speeds. Journal of Experimental Biology [Internet]. 2013 Jun 1;216(11):2150–60. Available from: http://jeb.biologists.org/cgi/doi/10.1242/jeb.075697

35. Buchanan TS, Lloyd DG, Manal K, Besier TF. Neuromusculoskeletal modeling: estimation of muscle forces and joint moments and movements from measurements of neural command. J Appl Biomech [Internet]. 2004 Nov;20(4):367–95. Available from: http://www.ncbi.nlm.nih.gov/pubmed/16467928

36. Nuckols RW, Dick TJM, Beck ON, Sawicki GS. Ultrasound imaging links soleus muscle neuromechanics and energetics during human walking with elastic ankle exoskeletons. Sci Rep [Internet]. 2020;10(1):1–15. Available from: http://dx.doi.org/10.1038/s41598-020-60360-4

37. Zajac FE. Muscle and tendon: properties, models, scaling, and application to biomechanics and motor control. Crit Rev Biomed Eng [Internet]. 1989;17(4):359–411. Available from: http://www.ncbi.nlm.nih.gov/pubmed/2676342

38. Johnson MA, Polgar J, Weightman D, Appleton D. Data on the distribution of fibre types in thirty-six human muscles. J Neurol Sci [Internet]. 1973 Jan;18(1):111–29. Available from: https://linkinghub.elsevier.com/retrieve/pii/0022510X73900233

39. Leitner C, Jarolim R, Englmair B, Kruse A, Hernandez KAL, Konrad A, et al. A Human-Centered Machine-Learning Approach for Muscle-Tendon Junction Tracking in Ultrasound Images. IEEE Trans Biomed Eng. 2021 Jun 1;

bioRxiv preprint doi: https://doi.org/10.1101/2025.08.20.671067; this version posted August 25, 2025. The copyright holder for this preprint (which was not certified by peer review) is the author/funder, who has granted bioRxiv a license to display the preprint in perpetuity. It is made available under a CC-BY 4.0 International license.

40. Ritsche P, Seynnes O, Cronin N. DL_Track_US: a python package to analyse muscle ultrasonography images. J Open Source Softw. 2023 May 2;8(85):5206.

41. Cronin N. Automated Analysis of Musculoskeletal Ultrasound Images Using Deep Learning. 2020.

42. Frangi AF, Niessen WJ, Vincken KL, Viergever MA. Multiscale vessel enhancement filtering. In 1998. p. 130–7.

43. Ryan DS, Stutzig N, Siebert T, Wakeling JM. Passive and dynamic muscle architecture during transverse loading for gastrocnemius medialis in man. J Biomech. 2019 Mar 27;86:160–6.

44. Blazevich AJ, Gill ND, Zhou S. Intra- and intermuscular variation in human quadriceps femoris architecture assessed in vivo. J Anat. 2006;209(3):289–310.

45. Ward SR, Eng CM, Smallwood LH, Lieber RL. Are current measurements of lower extremity muscle architecture accurate? Clin Orthop Relat Res. 2009;467(4):1074–82.

46. Martin JA, Brandon SCE, Keuler EM, Hermus JR, Ehlers AC, Segalman DJ, et al. Gauging force by tapping tendons. Nat Commun. 2018 Dec 1;9(1).

47. Handsfield GG, Meyer CH, Hart JM, Abel MF, Blemker SS. Relationships of 35 lower limb muscles to height and body mass quantified using MRI. J Biomech. 2014;47(3):631–8.

48. Roy RR, Meadows ID, Baldwin KM, Edgerton VR. Functional significance of compensatory overloaded rat fast muscle. J Appl Physiol. 1982 Feb 1;52(2):473–8.

49. Spector SA, Gardiner PF, Zernicke RF, Roy RR, Edgerton VR. Muscle Architecture and Force-Velocity Characteristics of Cat Soleus and Medial Gastrocnemius: Implications for Motor Control. Vol. 44. 1980.

50. Arnold EM, Ward SR, Lieber RL, Delp SL. A Model of the Lower Limb for Analysis of Human Movement. Ann Biomed Eng. 2010 Feb 3;38(2):269–79.

51. Azizi E, Roberts TJ. Muscle performance during frog jumping: Influence of elasticity on muscle operating lengths. Proceedings of the Royal Society B: Biological Sciences. 2010;277(1687):1523–30.

52. Otten E. A myocybernetic model of the jaw system of the rat. J Neurosci Methods [Internet]. 1987 Oct;21(2–4):287–302. Available from: https://linkinghub.elsevier.com/retrieve/pii/0165027087901233

53. Millard M, Uchida T, Seth A, Delp SL. Flexing Computational Muscle: Modeling and Simulation of Musculotendon Dynamics. J Biomech Eng. 2013 Feb 1;135(2).

54. Lee SSM, Arnold AS, Miara M de B, Biewener AA, Wakeling JM. Accuracy of gastrocnemius muscles forces in walking and running goats predicted by one-element and two-element Hill-type models. J Biomech. 2013 Sep 3;46(13):2288–95.

55. Wakeling JM, Lee SSM, Arnold AS, de Boef Miara M, Biewener AA. A muscle's force depends on the recruitment patterns of its fibers. Ann Biomed Eng [Internet]. 2012 Aug;40(8):1708–20. Available from: https://www.ncbi.nlm.nih.gov/pmc/articles/PMC3624763/pdf/nihms412728.pdf

bioRxiv preprint doi: https://doi.org/10.1101/2025.08.20.671067; this version posted August 25, 2025. The copyright holder for this preprint (which was not certified by peer review) is the author/funder, who has granted bioRxiv a license to display the preprint in perpetuity. It is made available under a CC-BY 4.0 International license.

56. Pataky TC, Vanrenterghem J, Robinson MA. Zero- vs. one-dimensional, parametric vs. non-parametric, and confidence interval vs. hypothesis testing procedures in one-dimensional biomechanical trajectory analysis. J Biomech. 2015;48(7):1277–85.

57. Statistical Parametric Mapping [Internet]. Elsevier; 2007. Available from: https://linkinghub.elsevier.com/retrieve/pii/B9780123725608X50001

58. Sawicki GS, Robertson BD, Azizi E, Roberts TJ. Timing matters: Tuning the mechanics of a muscle-tendon unit by adjusting stimulation phase during cyclic contractions. Journal of Experimental Biology. 2015 Oct 1;218(19):3150–9.

59. Bohm S, Marzilger R, Mersmann F, Santuz A, Arampatzis A. Operating length and velocity of human vastus lateralis muscle during walking and running. Sci Rep [Internet]. 2018;8(1):1–10. Available from: http://dx.doi.org/10.1038/s41598-018-23376-5

60. Voloshina AS, Kuo AD, Daley MA, Ferris DP. Biomechanics and energetics of walking on uneven terrain. Journal of Experimental Biology. 2013 Nov;216(21):3963–70.

61. Sloot LH, van den Noort JC, van der Krogt MM, Bruijn SM, Harlaar J. Can treadmill perturbations evoke stretch reflexes in the calf muscles? PLoS One. 2015;10(12).

62. Noorkoiv M, Stavnsbo A, Aagaard P, Blazevich AJ. In vivo assessment of muscle fascicle length by extended field-of-view ultrasonography. J Appl Physiol [Internet]. 2010 Dec;109(6):1974–9. Available from: https://www.physiology.org/doi/10.1152/japplphysiol.00657.2010

63. Bolsterlee B, Veeger HEJ, van der Helm FCT, Gandevia SC, Herbert RD. Comparison of measurements of medial gastrocnemius architectural parameters from ultrasound and diffusion tensor images. J Biomech. 2015 Apr 13;48(6):1133–40.

64. Blemker SS, Delp SL. Rectus femoris and vastus intermedius fiber excursions predicted by three-dimensional muscle models. J Biomech. 2006;39(8):1383–91.

65. Brennan SF, Cresswell AG, Farris DJ, Lichtwark GA. In vivo fascicle length measurements via B-mode ultrasound imaging with single vs dual transducer arrangements. J Biomech. 2017 Nov 7;64:240–4.

66. Lieber RL, Fridfin J. Muscle damage is not a function of muscle force but active muscle strain. 1993.

67. Perreault EJ, Heckman CJ, Sandercock TG. Hill muscle model errors during movement are greatest within the physiologically relevant range of motor unit firing rates. J Biomech. 2003;36(2):211–8.

68. Sandercock TG, Heckman CJ. Force From Cat Soleus Muscle During Imposed Locomotor-Like Movements: Experimental Data Versus Hill-Type Model Predictions. J Neurophysiol [Internet]. 1997 Mar 1;77(3):1538–52. Available from: https://www.physiology.org/doi/10.1152/jn.1997.77.3.1538

69. Umberger BR, Gerritsen KGM, Martin PE. A model of human muscle energy expenditure. Comput Methods Biomech Biomed Engin. 2003;6(2):99–111.

bioRxiv preprint doi: https://doi.org/10.1101/2025.08.20.671067; this version posted August 25, 2025. The copyright holder for this preprint (which was not certified by peer review) is the author/funder, who has granted bioRxiv a license to display the preprint in perpetuity. It is made available under a CC-BY 4.0 International license.

70. Holt NC, Azizi E. What drives activation-dependent shifts in the force-length curve? Biol Lett [Internet]. 2014 Sep 24;10(9):20140651–20140651. Available from: http://rsbl.royalsocietypublishing.org/cgi/doi/10.1098/rsbl.2014.0651

71. Close RI. The relations between sarcomere length and characteristics of isometric twitch contractions of frog sartorius muscle. J Physiol [Internet]. 1972 Feb 1;220(3):745–62. Available from: https://onlinelibrary.wiley.com/doi/10.1113/jphysiol.1972.sp009733

72. Huijing PA. Muscle, the motor of movement: properties in function, experiment and modelling. Vol. 8, Journal of Electromyography and Kinesiology. 1998.

73. Brown IE, Cheng EJ, Loeb GE. Measured and modeled properties of mammalian skeletal muscle. II. The effects of stimulus frequency on force-length and force-velocity relationships. J Muscle Res Cell Motil [Internet]. 1999 Oct;20(7):627–43. Available from: http://www.ncbi.nlm.nih.gov/pubmed/10672511

74. Libby T, Chukwueke C, Sponberg S. History-dependent perturbation response in limb muscle. Journal of Experimental Biology. 2020;223(1).

75. de Groote F, Allen JL, Ting LH. Contribution of muscle short-range stiffness to initial changes in joint kinetics and kinematics during perturbations to standing balance: A simulation study. J Biomech [Internet]. 2017;55:71–7. Available from: http://dx.doi.org/10.1016/j.jbiomech.2017.02.008

76. Lee HD, Herzog W. Force depression following muscle shortening of voluntarily activated and electrically stimulated human adductor pollicis. Journal of Physiology. 2003;551(3):993–1003.

77. Hamner SR, Seth A, Delp SL. Muscle contributions to propulsion and support during running. J Biomech [Internet]. 2010;43(14):2709–16. Available from: http://dx.doi.org/10.1016/j.jbiomech.2010.06.025

78. Arnold EM, Delp SL. Fibre operating lengths of human lower limb muscles during walking. Philosophical Transactions of the Royal Society B: Biological Sciences. 2011;366(1570):1530–9.

79. Ackland DC, Lin YC, Pandy MG. Sensitivity of model predictions of muscle function to changes in moment arms and muscle-tendon properties: A Monte-Carlo analysis. J Biomech [Internet]. 2012;45(8):1463–71. Available from: http://dx.doi.org/10.1016/j.jbiomech.2012.02.023

80. Pizzolato C, Lloyd DG, Sartori M, Ceseracciu E, Besier TF, Fregly BJ, et al. CEINMS: A toolbox to investigate the influence of different neural control solutions on the prediction of muscle excitation and joint moments during dynamic motor tasks. J Biomech [Internet]. 2015 Nov 5;48(14):3929–36. Available from: http://dx.doi.org/10.1016/j.jbiomech.2015.09.021

81. Willson AM, Anderson AJ, Richburg CA, Muir BC, Czerniecki J, Steele KM, et al. Full body musculoskeletal model for simulations of gait in persons with transtibial amputation. Comput Methods Biomech Biomed Engin [Internet]. 2022 May 2;1–12. Available from: https://www.tandfonline.com/doi/full/10.1080/10255842.2022.2065630

82. Lin CCK, Crago PE. Neural and mechanical contributions to the stretch reflex: A model synthesis. Ann Biomed Eng. 2002;30(1):54–67.

bioRxiv preprint doi: https://doi.org/10.1101/2025.08.20.671067; this version posted August 25, 2025. The copyright holder for this preprint (which was not certified by peer review) is the author/funder, who has granted bioRxiv a license to display the preprint in perpetuity. It is made available under a CC-BY 4.0 International license.

83. Lin CCK, Crago PE. Structural model of the muscle spindle. Ann Biomed Eng. 2002;30(1):68–83.

84. Blum KP, Lamotte D'Incamps B, Zytnicki D, Ting LH. Force encoding in muscle spindles during stretch of passive muscle. Ayers J, editor. PLoS Comput Biol [Internet]. 2017 Sep 25;13(9):e1005767. Available from: http://dx.plos.org/10.1371/journal.pcbi.1005767

bioRxiv preprint doi: https://doi.org/10.1101/2025.08.20.671067; this version posted August 25, 2025. The copyright holder for this preprint (which was not certified by peer review) is the author/funder, who has granted bioRxiv a license to display the preprint in perpetuity. It is made available under a CC-BY 4.0 International license.

Supplementary Figures

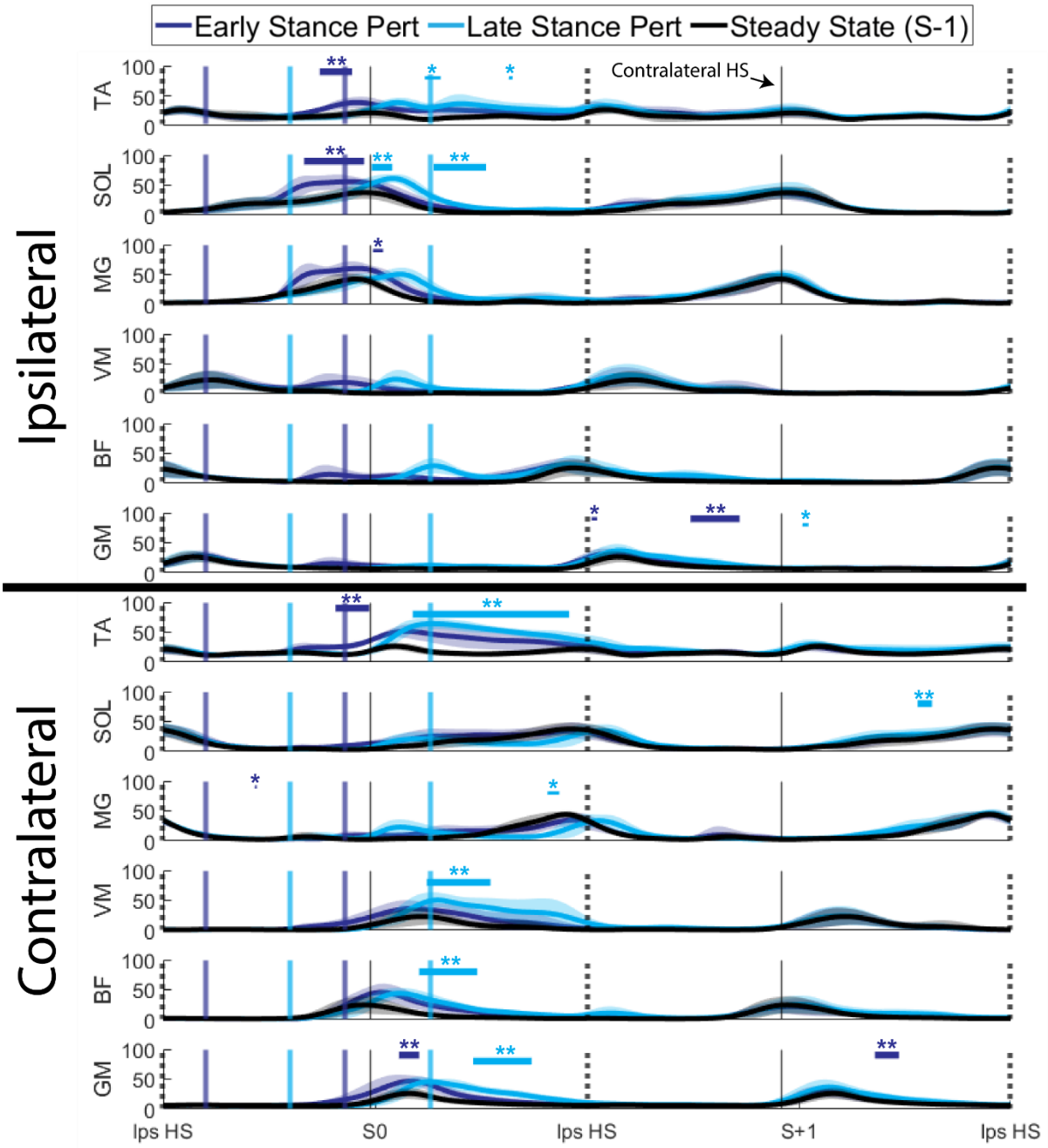


Figure S1 – Muscle activations (% max across all trials) on both legs relative to the perturbation across all participants (n=7, 222 perturbations), time-normalized to gait cycles. TA = tibialis anterior, SOL = soleus, MG = medial gastrocnemius, VM = vastus medialis, BF =biceps femoris, GM = gluteus maximus. Shaded regions represent ±1 standard deviation. Instances when curves significantly deviated from steady state (S-1) are identified with thick horizontal lines and ** for $p < 0.001$, and thin horizontal lines and * for $p < 0.05$. Solid colored vertical lines indicate average start and end times of the perturbations. Dotted/solid black vertical lines indicate instances of ipsilateral/contralateral heelstrike, respectively. "Steady State" strides were the strides preceding the perturbed stride (S-1).

bioRxiv preprint doi: https://doi.org/10.1101/2025.08.20.671067; this version posted August 25, 2025. The copyright holder for this preprint (which was not certified by peer review) is the author/funder, who has granted bioRxiv a license to display the preprint in perpetuity. It is made available under a CC-BY 4.0 International license.

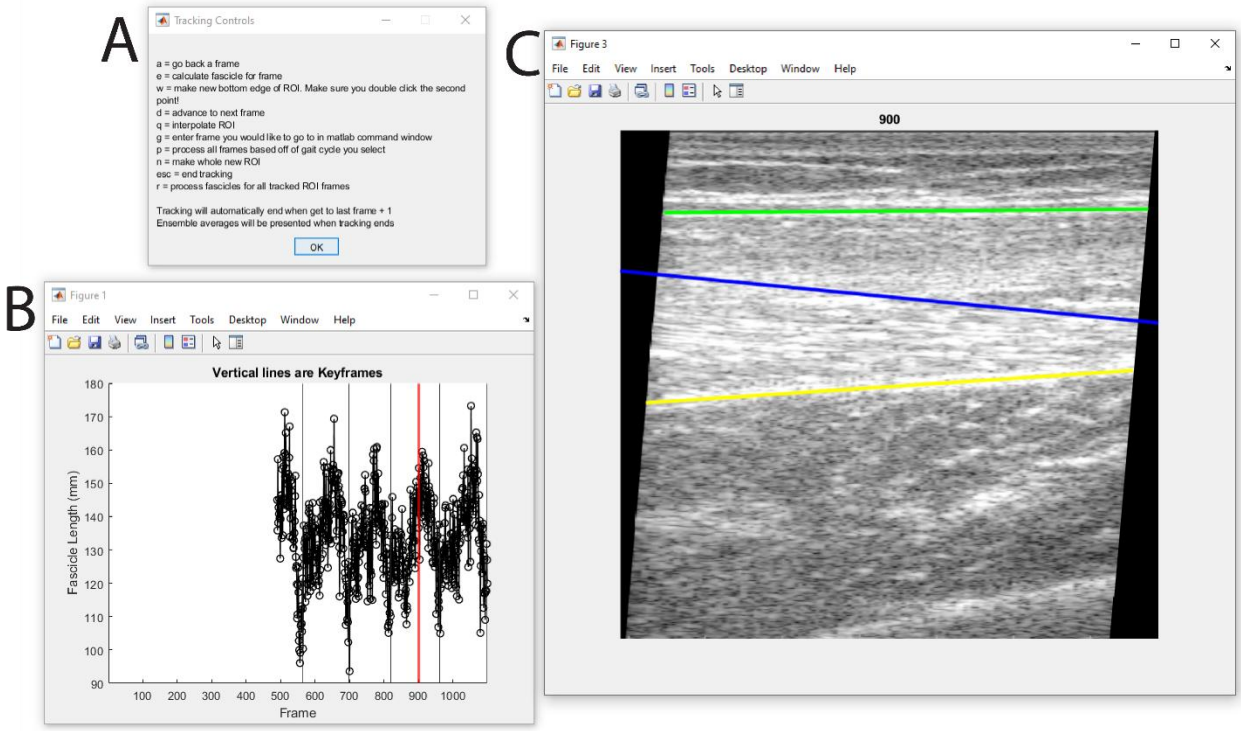


Figure S2 - Custom fascicle tracking application user interface. A) Instructional information for operating the tracker. B) Representative fascicle length window. The vertical red line indicates the current image frame. Vertical thin black lines indicate keyframes (*e.g.* ipsilateral heelstrikes). C) Image window. The green line indicates the superficial aponeurosis, the yellow line indicates the deep aponeurosis, and the blue line is a graphical presentation of a representative fascicle located at the middle of the images.

bioRxiv preprint doi: https://doi.org/10.1101/2025.08.20.671067; this version posted August 25, 2025. The copyright holder for this preprint (which was not certified by peer review) is the author/funder, who has granted bioRxiv a license to display the preprint in perpetuity. It is made available under a CC-BY 4.0 International license.

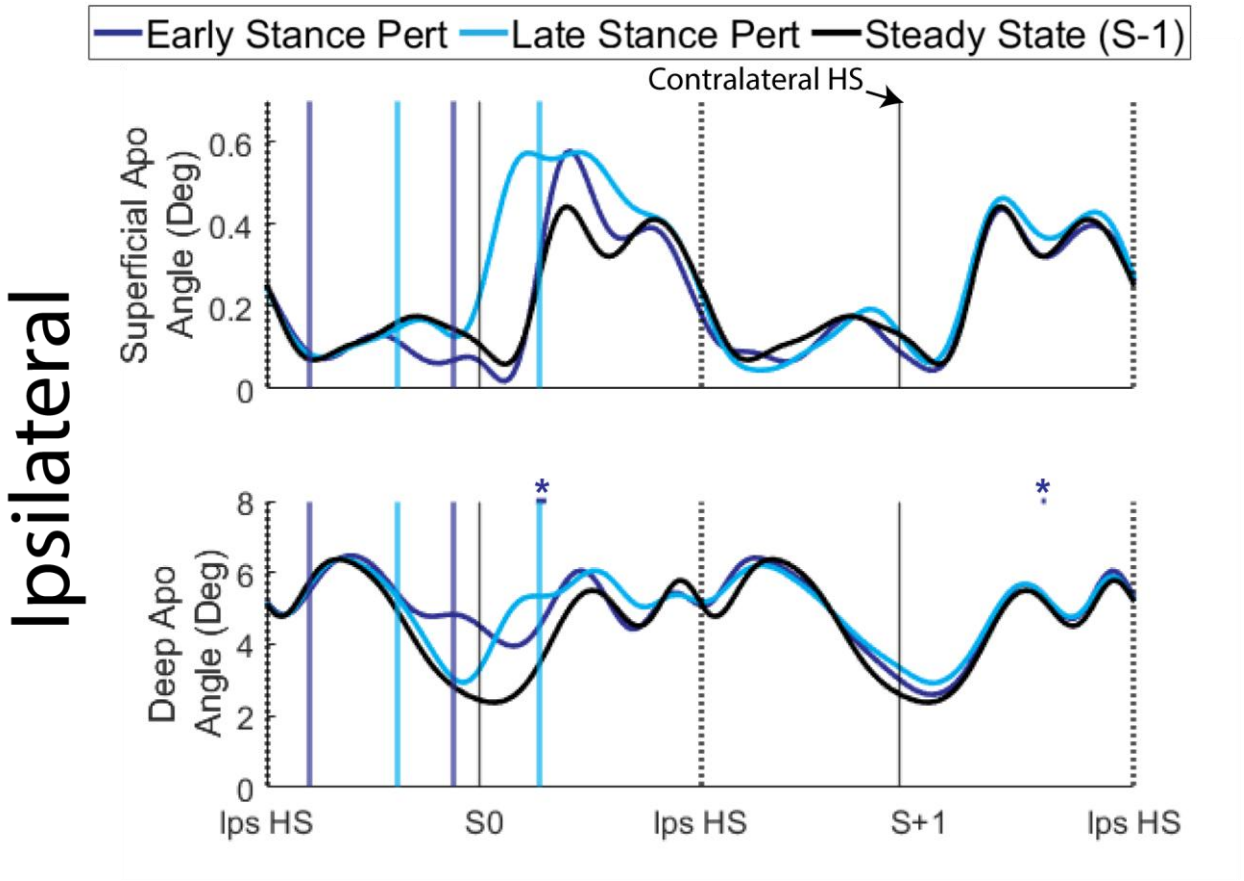


Figure S3 – Superficial and deep aponeurosis angles relative to horizontal (positive is counterclockwise) on the ipsilateral leg relative to the perturbation across all participants (n=7, 222 perturbations), time-normalized to gait cycles. Standard deviations are omitted for clarity. Instances when curves significantly deviated from steady state (S-1) are identified with thick horizontal lines and ** for $p < 0.001$, and thin horizontal lines and * for $p < 0.05$. Solid colored vertical lines indicate average start and end times of the perturbations. Dotted/solid black vertical lines indicate instances of ipsilateral/contralateral heelstrike, respectively. "Steady State" strides were the strides preceding the perturbed stride (S-1).